MADRID
inter.noise 2019
June 16 - 19
NOISE CONTROL FOR A BETTER ENVIRONMENT

Influence of sound reflection on aircraft directivity and lateral attenuation on the ground

Amargianitakis, Daniel C. [1], Self, Rod H. [2], Torija, Antonio J. [3], Synodinos, Athanasios P. [4]

ABSTRACT

The calculation of the lateral attenuation correction for computing aircraft noise footprints on the ground, as proposed by Doc29 and AIR5662, is based on semiempirical methods not suitable for accounting for the particular characteristics of some of the novel aircraft designs under study; involving new configurations and propulsion and power systems. The lateral attenuation correction is known to depend on three factors: engine installation e_ects, ground absorption, and refraction and scattering of the sound. This study aims to numerically calculate the e_ects of the sound produced by the aircraft main sources (fan, jet) when reflected and scattered o_ of the wing, tail-plane surfaces and the fuselage of the aircraft. A simple 3D model geometry was used, approximating that of an A320, a MD11 and a MD83. Subsequently modelling the main sound sources as acoustic monopoles and using ray theory, a sound directivity field around the aircraft was calculated, which in turn was propagated to the ground. Then employing typical constant altitude flyovers, the Sound Exposure Level (SEL) were calculated and compared to an equivalent spherically symmetric source. It is shown that aircraft directivity is highly dependant on the nature of noise sources, their position relative to reflective surfaces and the geometry of those surfaces.

Keywords: Aircraft Noise, Sound Reflection, Aircraft Directivity, Lateral attenuation
I-INCE Classification of Subject Number: 76

1. INTRODUCTION

The traditional noise sources encountered on conventional aircraft are reasonably well understood, and are discussed is detail by Synodinos [1]. The already existing literature and semi-empirical models, [2], [3] may no longer apply as the introduction of novel technologies such as hybrid or fully electric propulsion systems alter sound emission significantly. Also, the development of urban air mobility vehicles suggests that new configurations of propeller driven vehicles with different flight procedures, could increase the number and alter the characteristics of noise sources. Therefore new tools for calculating the directivity of the overall air vehicles need to be developed. This paper aims to introduce a framework, currently under development, for the computation of sound directivity of unconventional aircraft designs and presents the results of lateral directivity of a simplified (contemporary) aircraft model based on frame reflections alone.

At this stage, source directivity, atmospheric absorption and ground e_ects are not taken into account.

[1]dca1g14@soton.ac.uk
[2]rhs@soton.ac.uk
[3]A.J.Martinez@soton.ac.uk
[4]A.Synodinos@soton.ac.uk

2. THEORETICAL BACKGROUND

2.2.1. Directivity

Directivity of a source is defined as a ratio of intensities (1) which reveal how a directional source concentrates the available power in a specific direction.

$$D(\theta, \phi) = \frac{I(\theta, \phi)}{\bar{I}} \tag{1}$$

$D(\theta, \phi)$, known as the directivity factor, is expressed in terms of polar and azimuthal angles (θ, ϕ) defined in Figure 1, where I is the intensity in the specified direction and $\bar{I}$ is the intensity of a spherically symmetric source of equivalent sound power .

Despite each individual source of noise on an aircraft (jet, fan, frame, landing gear etc) having an individual directivity associated with it, the aircraft overall directivity is identified approximately as an omnidirectional, for conventional turbofan designs. This does not hold for rotorcraft, as propellers inherently have an directivity associated with them. As concepts of future novel aircraft continue to appear, propellers will have a dominant presence, especially for urban ore very short-haul designs, with arrays of them being positioned in different configurations to allow for the desired characteristics, as for example distributed propulsion systems. These configurations will naturally differ in terms of directivity from the conventional setup.

In this paper we assume that the aircraft directivity is a function of only airframe reflections of an conventional setup. The sound pressure level given in terms of sound power is:

$$L_p(\theta, \phi, r) = 10 \log_{10} \left[\frac{WD(\theta, \phi)}{r^2} C \right] \tag{2}$$

where $C = \rho c/(4\pi p_{ref}^2)$. If we assume our radius, r, to be at a reference value of $r_{ref} = 1$ and take the difference with the equivalent sound pressure level of a spherically symmetric source at the same radius, we have :

$$dL_p(\theta, \phi) = 10 \log_{10} \left[D(\theta, \phi) \right] \tag{3}$$

as $D(\theta, \phi)$ for a spherically symmetric source is by definition 1. Therefore by calculating $dL_p(\theta, \phi)$ we can directly assess the overall and lateral directivity of an aircraft.

2.2.2. Lateral Attenuation

AIR5662 and Doc29, [4], [5] define Lateral Attenuation as, the attenuation, not attributed to atmospheric absorption or wave divergence (geometric spreading), of sound propagating from a sound source located on an aircraft, to a receiver at a location to the side of the flight path. It is usually accounted for as a correction term when computing aircraft noise contours. It is expressed in decibels. It is important to distinguish between instantaneous and averaged quantities. In the context of this paper, instantaneous sound pressure levels are calculated and their effects are integrated over time as a linear flyover is employed, to get the cumulative effects. To maintain conventions the co-ordinate system and variables defined in this section will follow that of Krebs in [6]. Lateral Attenuation is defined using three main variables, ℓ_0 the lateral distance between the receiver and the aircraft (minimum slant distance), ε the aircraft bank angle and β the aircraft elevation angle. In this study ε is assumed to be zero, and therefore neglected. The system of coordinates and definitive angles are presented in Figure 1.

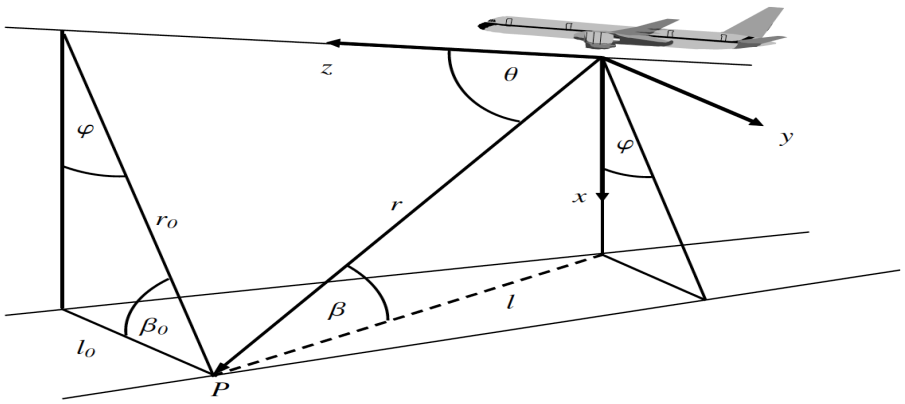

Figure 1: Coordinate system used, as in Doc29 [5] and Krebs [6]

Lateral Attenuation is attributed to some key physical mechanisms, engine-installation effects, absorption by the ground surface and refraction and scattering of the sound signal from wind and meteorological conditions. All three of these mechanisms have been studied in the past either in an empirical manner or a theoretical one. The methods described in AIR5662 [4] for calculating the correction terms are based on data collected from routine aircraft operations and flight tests. This allowed for the key parameters to be determined. In terms of engine-installation effects three main configurations (categories) of aircraft have been distinguished: wing mounted, fuselage mounted and propeller driven. As stated in AIR5662, ground effects have been thoroughly researched and are reasonably well understood. Finally, refraction and scattering effects have been modelled using the quantification of the other two parameters and subtraction from the overall sound levels encountered, see [4] for further details. Lateral Attenuation is calculated using:

$$\Lambda(\beta, \ell) = \Gamma(\ell)\Lambda(\beta) \tag{4}$$

where $\Gamma(\ell)$ is a distance factor, and $\Lambda(\beta)$ is long-range air-to-ground lateral attenuation given in AIR5662 [4].

These expressions are assumed to hold for all the cases of aircraft, and form the more general solution to the calculation of lateral attenuation. It is worth noting that the term $\Lambda(\beta)$ does not account for lateral directivity. Using the assumptions already discussed, a total lateral adjustment $\Lambda_T(\beta, \ell)$ is defined as the sum of lateral attenuation and lateral directivity, $\Delta(\beta)$, as:

$$\Lambda_T(\beta, \ell) = \Lambda(\beta, \ell) + \Delta(\beta) \tag{5}$$

which can be rearranged to give the lateral attenuation. Lateral directivity correction factor is different for the three types of aircraft mentioned above, i.e. wing-mounted, fuselage-mounted and propeller. The equations hold for the generalised assumption, that the sound is arriving at the observer point from an aircraft in steady level flight performing an flyover along an infinite path. This report calculates the lateral directivity associated with reflections off the fuselage and wing:

$$\Delta(\beta) = dL_p(\theta, \phi) = 10 \log_{10} [D(\theta, \phi)] \tag{6}$$

3. 3D REFLECTION NUMERICAL MODEL

The numerical method presented in this section is a high frequency approximation using ray theory. The geometry used to approximate the three different aircraft types is built up of simple shapes; namely: a circular cylinder for the fuselage and finite planar sections for the wings. The sources are modelled as acoustic monopoles positioned at the average location of sound generation of a conventional turbofan engine.

A rigid cylinder of radius a and of length L is placed at the origin. The cylinder axis is aligned with the x-axis (This was chosen as it complies with the analytical model used for verification; an axis rotation was later performed to return to Figure 1 system). A quiescent medium (fluid) is considered. The monopole source $\mathbf{S} = (x_S = 0, y_S = |\bar{\rho_0}|, z_S)$ is located on the $y - z$ plane, along the y-axis defined by the position vector, $\bar{\rho_0}$.

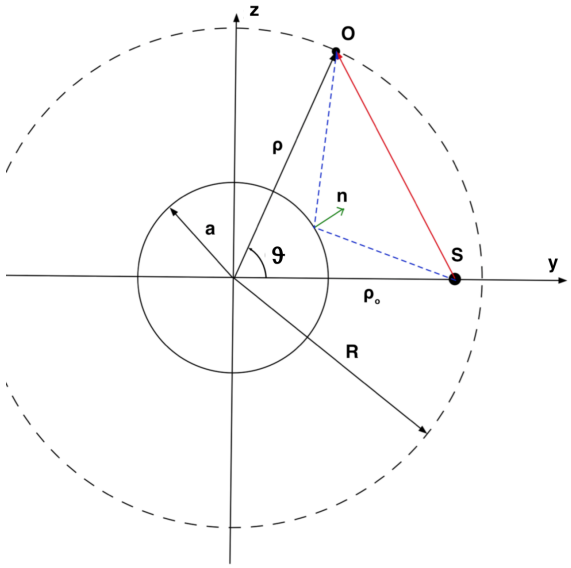

Figure 2: $y - z$ plane of Circular Cylindrical geometry

The method of images is used for the problem of sound reflection. The method of image sources supposes a perfectly rigid plane. A boundary condition of zero normal velocity of the fluid is assumed, meaning that normal pressure gradient is zero. This can be accomplished by imagining a continuation of the medium behind the reflective plane, as a mirror image of the of the real field. The reflective plane acts as a symmetry plane, therefore we may replace the effects of the boundary plane by a set of image sources, placed symmetrically with respect to the boundary plane, with both source and its image radiating into un bounded space. Of course only the region outside of the boundary plane contains the medium and carries acoustic energy.

In the case of the finite circular cylinder, we define the circumference of said cylinder by number of points N, and the length by a number of points M. Each point on the circumference has an associated unit normal vector $\bar{n}$. Each of these unit normal vectors defines a plane of which reflection happens. As a consequence each unit normal vector has its own image source associated with it. Moving along the length of the cylinder (constant ϑ) the unit normal vector of the surface is constant, as the two principal radii of curvature at the surface of a cylinder are $R_C = a$ and ∞. The position of these image sources is therefore a function of the curvature of the surface and vary only as a function of the polar angle ϑ. The position of these image sources can then be defined as follows:

First of all, we define the points T_1, T_2 on the circumference of the circular cylinder, as the points of tangency between the circular cylinder and the two lines passing through the position of the source. This defines the illuminated region of the cylinder and the shadow region respectively.

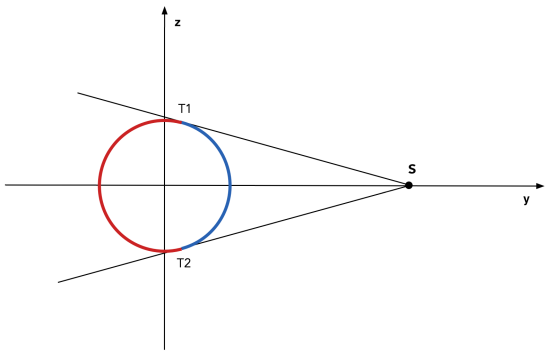

Figure 3: Illuminated and shadow regions of Cylinder

For all the points in the shadow regions, there is no image source defined as no direct ray of sound ever reaches them, and therefore reflection does not occur. In the illuminated region, a separate image source is defined for points around the circumference at different polar angles, but points along a line parallel to the cylinder centreline defined by a constant polar angle ϑ all have the same image source.

The position of the image at each angle ϑ is calculated as:

We define the vector $\bar{v}$ as the vector originating at the position of source S and ending at our point C on the cylinder circumference in the illuminated region:

$$\bar{v} = C - S \tag{7}$$

We can now find the distance between the source S and the reflective plane defined by the unit normal vector at point C. This is:

$$d = |\bar{v} \cdot \bar{n}| \tag{8}$$

Therefore the image source is positioned on the line defined by the source S and the unit normal vector at a distance $2d$ from S.

$$I = S - 2d\bar{n} \tag{9}$$

We can now note that all image sources, defined by the surface of the circular cylinder, are positioned in the $x = x_s = 0$ plane as they are a function of the cylinder curvature.

In the 2D plane, $x = 0$ for example, each of the image sources will define a single reflected ray that will pass through the point C they were defined with. We define the reflected ray by its origin I, the image source and the direction vector (slope) D.

In three dimensional space a single image source will define multiple reflected rays, directly equal to discretisation points M along the length of the cylinder. Each reflected ray has the same origin, but a different direction depending on the position of point C along the length of the cylinder.

$$D_m = C_m - I \tag{10}$$

where subscript m is a counter defined : $1 \leq m \leq M$. Therefore, each image source produces a fan of reflected rays passing through the surface of the cylinder, Fig 5

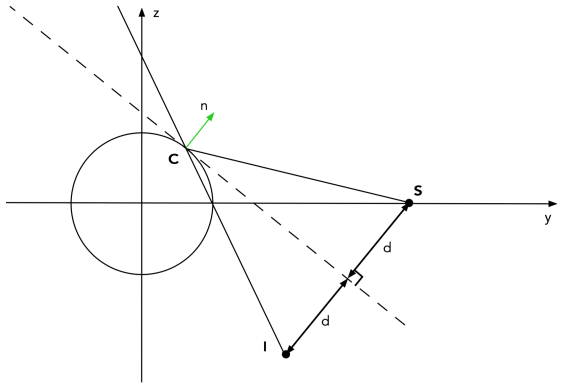

Figure 4: Image source position I, as defined by $\bar{n}$ and S

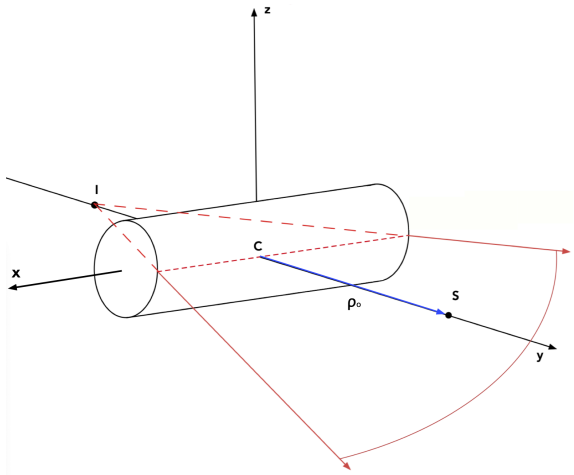

Figure 5: Fan of reflected rays as generated from the image source, passing through the cylinder surface

3.3.1. Directivity sphere generation

Observer positions on the sphere are defined by $\mathbf{O} = (x_O, y_O, z_O)$ or the position vector $\bar{\rho}$.

We define the surface of a sphere in parametric form, with the centre at the origin. The sphere surface is defined in three-dimensional cartesian coordinates as:

$$x^2 + y^2 + z^2 = \rho^2 \tag{11}$$

The actual position of the observer will be determined by finding the intersection of the reflected ray and the sphere surface. We can solve for the x, y and z location of the observer point on the circle using a parametric representation of the coordinates. So for the reflected ray $R_r(t)$, defined as a vector of origin I the image source, and direction $\bar{D_m}$:

$$\bar{R_r}(t) = I + t\bar{D_m} \tag{12}$$

Inserting this into the Equation 11 for the observer sphere, we form a quadratic equation for t. Substituting the roots t_1, t_2 into the vector Equation 12, we get the location of two points on the observer sphere. The correct observer location O for this particular solution is the point which follows the positive direction of D_m along the line.

3.3.2. Pressure Fields and correction for reflection from curved surfaces

We have now defined a series of observer locations on the sphere of radius ρ which see a reflected ray. These points also define an illuminated and shadow region on the observer circle. The points in the shadow region, do not see any rays at all, therefore the pressure field is assumed to be equal to the reference pressure $p_{ref} = 20 \cdot 10^{-6}$. The points in the illuminated region also see a direct ray from the source S. Therefore we can calculate the direct and reflected pressure fields as:

$$p_d = \frac{A}{r} e^{-ikr} \tag{13}$$

where A is the amplitude of the spherical pressure wave, r the distance of the observer to the source given by:

$$r = \sqrt{(x_S - x_O)^2 + (y_S - y_O)^2 + (z_S - z_O)^2} \tag{14}$$

We therefore have:

$$\sqrt{|p_d|^2} = \sqrt{|\frac{A}{r} e^{-ikr}|^2} = \sqrt{|\frac{A}{r}|^2} \tag{15}$$

3.3.3. Ray Acoustics and Reflection from curved surfaces correction

When working in terms of ray acoustics, the notions of a ray-tube and ray-tube areas are used. This idea is useful in capturing the variation of the wave amplitude along rays. A ray-tube may be considered as all the rays passing through a tiny area $A(x_0)$ centred at x_0 transverse to the ray path (with the ray path being from x_0, the point of origin, to a random observer location x). When the ray tube reaches x, its cross-sectional area will be $A(x)$. Therefore we can write an expression connecting the wave amplitude to the ratio of the ray-tube area:

$$p_r(x) = p(x_0) \left[\frac{A(x_0)}{A(x)} \right]^{1/2} \tag{16}$$

In the problem of reflecting sound off a cylinder, as ray-tube of area $A(x_0) = A(C)$ encounters a curved surface like that of the circular cylinder the area of this ray-tube will change due to the different radii of curvature encountered by the different rays in the tube. This results in a reflected ray-tube of area $A(x) = A(O)$ after subsequent propagation to the observer O, and for the specific case of reflecting a spherical wave off a circular cylinder Pierce [7] ,gives:

$$\frac{A(O)}{A(C)} = (1 + R_i^{-1} l)[1 + R_i^{-1} l + 2 l R_c^{-1} N(\phi_i, \theta_i)] \tag{17}$$

where $N(\phi_i, \theta_i)$ is given by

$$N(\phi_i, \theta_i) = \sin^2 \phi_i \sec \theta_i + \cos^2 \phi_i \cos \theta_i = \frac{1 - (n_i \cdot e_C)^2}{-n_s \cdot n_i} \tag{18}$$

where R_i is the incidents wave radius of curvature at the point C of reflection, R_C one of the principal radii of curvature of the cylinder, ϕ_i the angle between the plane of incidence and the line passing through the reflection point parallel to the cylinder axis, l the distance of propagation to the obeserver O after reflection, θ_i the angle of incidence at C and finally

n_i, n_S and e_C unit vector in the direction of incidence, unit normal vector at the point C and the unit vector parallel to the cylinder axis, respectively.

The wings of the 3D model approximations are treated at as planes of specific dimensions. We assume the reflection off the planar geometric is perfect, i.e the there is no transmission wave generated. The problem is again amenable to the method of images. The image source is introduced, with strength and location satisfy the boundary conditions of planar interface. This is accomplished by the same methodology described in Section 3.

The aircraft noise produced by the monopole source has been split in two contributions, that of the direct ray and the reflected ray. On top of that the summation of the two respective contributions from the second monopole source has to be considered. These contributions from the two sources producing pressures time averaged pressures $p_{1,d}, p_{1,r}, p_{2,d}$and $p_{2,r}$ at a point in space, added incoherently give a total pressure of:

$$p_T^2(\theta, \varphi) = p_{1,d}^2 + p_{1,r}^2 + p_{2,d}^2 + p_{2,r}^2 \tag{19}$$

It is worth noting that data calculated for pressures $p_{1,d}$ etc. is scattered on the surface of sphere, therefore linear interpolation was used in order to get $p_T^2(\theta, \varphi)$. The final product is a sphere of radius r_{ref} of the sound levels, representing of the directivity of the total modelled aircraft.

4. VALIDATION

This section describes the analytical method implemented in [8] to validate the numerical model described in the above sections. We are concerned about the reflections off a cylindrical fuselage, thus the solution we use is that of an infinite circular cylinder. Reflection of a spherical wave off a half-plane [8] was used to validate wing reflection, but for this paper it was omitted as it proved to be trivial compared to the more complicated reflection of a cylindrical surface.

The body in this case is considered to be two-dimensional as the surface is described by:

$$\rho = f(\phi), \qquad 0 \leq \phi \leq 2\pi \tag{20}$$

The problem is however not characterised as two-dimensional, as that depends on the nature of the source. Bowman produces two solutions, one general exact acoustical solution and one high frequency approximation (using geometric optics acoustics; the one used) for the scattered field from a circular cylinder with a monopole as the source of sound.

4.4.1. Analytic model description

In more detail the geometry used in the analytical model is the following: Using circular cylindrical coordinates (ρ, ϕ, z) related to Cartesian coordinates (x, y, z) by the transformation:

$$x = \rho \cos \phi, \tag{21}$$

$$y = \rho \sin \phi, \tag{22}$$

$$z = z. \tag{23}$$

where $0 \leq \rho \leq +\infty, -\infty \leq z \leq +\infty$. The z-axis is the symmetry axis and the surfaces $\rho = constant, \phi = constant$ and $z = constant$ are coaxial circular cylinders of radius ρ, half-planes originating in the z-axis, and planes perpendicular to the z-axis.

The reflective body is the surface defined by $\rho = a$, and the source used in this case is a point source (monopole), 24, located at $(\rho_0 \geq a, \phi_0 = 0, z_0 = 0)$.

So for a point source at $(\rho_0, \phi_0 = 0, z_0 = 0)$ for an acoustically hard cylinder, such that:

$$V^i = \frac{e^{ikR}}{kR} \tag{24}$$

the geometric optics scattered field at a point $(\rho, \phi < \pi, z)$ located in the illuminated region is:

$$V^s_{g.o.} = \frac{1}{k}\left\{(F^2 + z_1^2)(1 + \sqrt{G/F})\Big[1 + \frac{G}{K} + \frac{2G}{a\cos\phi_1 + \alpha}\Big]\right\}^{\frac{1}{2}} \times \exp\left\{ik\Big[\sqrt{F^2 + z_1^2} + \sqrt{G^2 + (z - z_1)^2}\Big]\right\} \tag{25}$$

where α, z_1, F, G and ϕ_1 are defined in [8] as functions of the spatial coordinates and geometry of the model. The symbols V^i and V^s are the incident and scattered velocity potentials respectively, with $V = V^i + V^s$. The geometric optics field is zero in the shadowed region, as is the numerical model. This is true of all points which satisfy the inequalities:

$$|\psi| > \arccos\frac{a}{\rho_0} \tag{26}$$

$$\rho < \rho_0[\cos\psi + \sqrt{(\rho_0/a)^2 - 1}\sin|\psi|]^{-1} \tag{27}$$

The acoustic pressure of the reflected and direct fields are recovered from the velocity potential by implementation of Newton's momentum equation for a fluid at rest and assuming harmonic vibrations:

$$p = i\omega\rho_0 V \tag{28}$$

Figure 6 shows the sound pressure level of the reflected ray calculated at observer locations on a circle of radius 1000m on the $x - y$ plane, as indicated in the diagram of Figure 2. The SPLs of the analytic solution agrees with the three-dimensional numerical model almost perfectly.

5. CUMULATIVE NOISE METRICS STUDY

A straight level flight at constant altitude H and velocity U was performed for different observer locations on the ground defined by the lateral angle φ. The complete time history of sound pressure level at the observer location were calculated using a time step method. For each discrete position of the aircraft the sound pressure level at the observer location is given by:

$$L_{model}(\varphi, \theta) = L_{model}|_{r_{ref}}(\varphi, \theta) - 20\log\frac{r}{r_{ref}} = L_{model}|_{r_{ref}} - 20\log r \tag{29}$$

Knowing the instantaneous sound levels at each of the time increments $\Delta T = 1$, the sound exposure levels (SEL) L_{AE} can also be determined:

$$L_{AE} = 10\log\Big(\frac{1}{T}\sum_{i=0}^{n} 10^{L_{model,i}/10}\Delta T\Big) \tag{30}$$

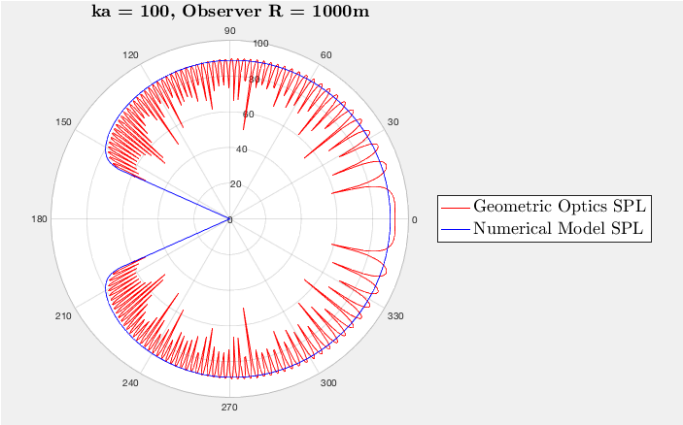

Figure 6: Comparison of the predicted and analytical pressure magnitude along the azimuthal angle in the $z = 0$ plane for the reflected field.

The same procedure can be applied to the spherically symmetric source in order to calculate the SEL.

In order to create an equivalent spherically symmetric model the acoustic power of the 3-D numerical model has to be calculated and matched to that of the spherically symmetric model. This is accomplished by averaging the $p_T^2(\theta, \varphi)$ values over the entire sphere and multiplying by the area of that sphere.

As seen in Figure 8, the observer locations are limited to the lateral angle values $\varphi \leq 70°$, this is because as discussed in [6] , the effects caused by ground effects are less important in this region and can be assumed to negligible. Therefore in this region, the differences observed between the two models can be attributed to the lateral directivity.

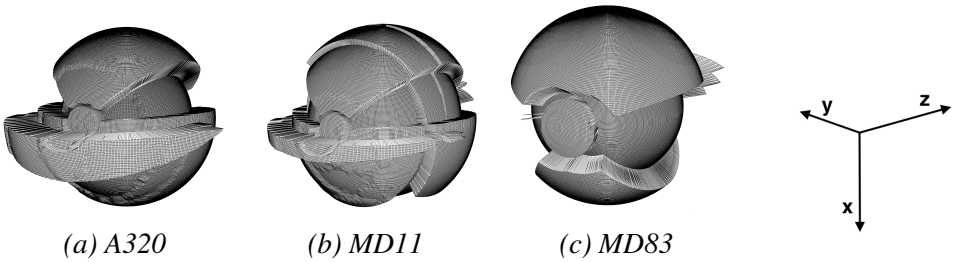

(a) A320 *(b) MD11* *(c) MD83*

Figure 7: Graphic representation of the directivity pattern resulting from the three different types of aircraft geometry. In this representation the radius of the sphere at any given point is proportional to the SPL. The orientation of the spheres are reversed, compared to Figure 1, in order to visualise the wing reflection which appears in the rear hemisphere for wing mounted engines.

The deviations between the 3D numerical model and the spherically symmetric source, in this case, are only due to the effects of reflections off of the cylindrical and planer geometry. As mentioned by Krebs [6], differences in lateral directivities can occur even when the geometry is kept constant; this could be attributed to the directivities of the individual sources. As this calculation assumed omnidirectional monopole sources positioned at average locations between the main aircraft engine sources (jet, fan), the discrepancies between the results presented in Figure 8 and Figure 4 in Krebs [6], can be directly related to the location of these monopoles relative to the reflective surfaces and the geometry (curvature, size etc.) of these reflective surfaces.

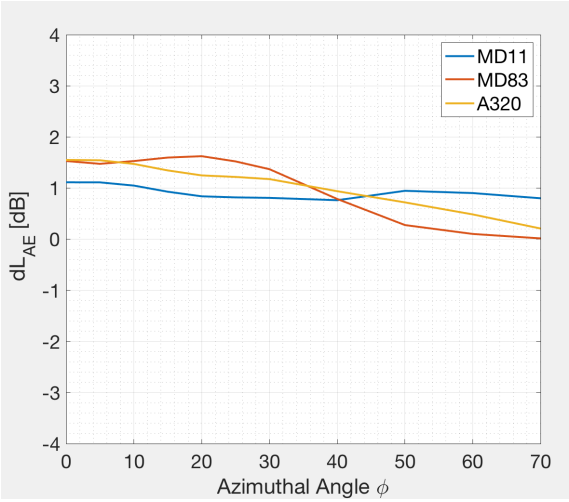

Figure 8: Lateral sound directivity of geometries approximating three different aircraft

As shown Figure 8, lateral directivity is heavily dependant on engine position relative to the reflective surfaces. Fuselage reflections seem to be the main contributors, as reflections are "visible" by observer locations for longer. Fuselage shielding effects also contribute largely towards decreasing the the sound levels in the shadowed regions. These effects are especially apparent in the case of the MD11, which has fuselage mounted engines, as shadows and reflected are directed towards the ground, while wing reflections can be neglected as they point towards the sky.

6. CONCLUSIONS

In this paper a three-dimensional ray theory model was created in order to assess how aircraft frame (wing and fuselage) effect the directivity of the overall aircraft, and in tern the lateral attenuation on the ground. The validity of the model was tested using a high frequency analytical solution of a monopole source scattered by an infinite circular cylinder. The numerical model displayed satisfying agreement with the reference analytical solutions, thus allowing for further calculations.

The numerical model consisted of generating a simplistic geometry of an aircraft frame using circular cylinder and tailored planes. The direct and reflected pressure fields were calculated on sphere of assumably infinite radius surrounding the aircraft. The reflected field was defined using the method of images were image sources are placed behind the surfaces of reflection. Shadow regions were treated as in the geometric optic solution and assumed to have a zero field. Thus resulting in a sphere (or equivalent sound source) for the entire aircraft.

As a result, flyovers of constant altitude and velocity were implemented to assess the lateral attenuation on the ground, in terms of Sound Exposure Levels. In order to evaluate the effect of the directivity of the equivalent source, results were compared with a spherically symmetric source of the same acoustical energy. Ground effects and atmospheric absorption were not concidered in this particular model.

According to the study of three different aircraft setups, one wing mounted (A320), one fuselage mounted (MD83) and finally one with both fuselage and wing mounted engines (MD11), it was determined that lateral directivity is highly sensitive to engine installations effects. The aircraft geometry also has a significant effect, especially the fuselage because

of its larger wetted area and its effect on the directivity in the azimuth angle direction. The results presented are in line with existing literature, showing an important change of the sound exposure level at the ground as a function of azimuthal angle. Further work will carried out to improve the accuracy of the definition of the sound sources, accounting for specific directivities of sources. Furthermore, the model will be upgraded to account for more sophisticated aircraft geometries.

7. REFERENCES

[1] A.P. Synodinos. *A new framework for estimating noise impact of novel aircraft*. PhD thesis, 2017.

[2] Society of automotive engineers: Procedure for the calculation of aircraft noise in the vicinity of airports. Technical Report 1845, SAE AIR, 1981.

[3] Prediction method for lateral attenuation of airplane noise during takeoff and landing. Technical Report SAE AIR-1751, Society of Automotive Engineers, 1981.

[4] Air-5662. Technical report, Society of Automotive Engineers, 2006.

[5] Report on standard method of computing noise contours around civil airports, vol. 2: Technical guide. Tech. rep. ecac.ceac doc. 29, 4th ed, European Civil Aviation Conference (ECAC), December 2005.

[6] W. Krebsand G. Thomann. Aircraft noise: Aspects on lateral sound attenuation. 95(1013 – 1023), 2009.

[7] A. D. Pierce. *Acoustics: an Introduction to its Physical Principles and Applications*. American Institute of Physics, 1989.

[8] T.B.A. Senior J.J Bowman and P.L.E. Uslenghi. *Electromagnetic and acoustic scattering by simple shapes*. Radiation Laboratory, The University of Michigan, Ann Arbor, Michigan, 1970.

[9] D. A. Bies and C. H. Hansen. *Engineering noise control*. Spon Press, 2009.

[10] A. B. Coppens L. E. Kinsler, A. R. Frey and J. V. Sanders. *Fundamentals of acoustics*. John Wiley and Sons, 4th edition, 2000.

[11] S. Pluss G. Thomann W. Krebs, R. Butikofer. Spectral three-dimensional sound directivity models for fixed wing aircraft. *Acta Acustica united with Acustica*, pages 269–277, 2006.